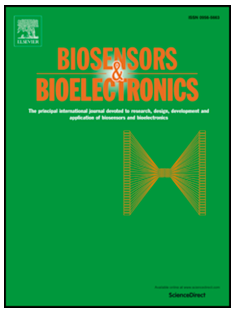

Coupling aptazyme and catalytic hairpin assembly for cascaded dual signal amplified electrochemiluminescence biosensing

Zhenqiang Ning, Yongjun Zheng, Deng Pan, Yuanjian Zhang, Yanfei Shen

PII: S0956-5663(19)31023-1

DOI: https://doi.org/10.1016/j.bios.2019.111945

Reference: BIOS 111945

To appear in: *Biosensors and Bioelectronics*

Received Date: 10 September 2019

Revised Date: 22 November 2019

Accepted Date: 30 November 2019

Please cite this article as: Ning, Z., Zheng, Y., Pan, D., Zhang, Y., Shen, Y., Coupling aptazyme and catalytic hairpin assembly for cascaded dual signal amplified electrochemiluminescence biosensing, *Biosensors and Bioelectronics* (2020), doi: https://doi.org/10.1016/j.bios.2019.111945.

ZN and YS(*), conceived and planned experiments. ZN prepared the nanocomposites, and performed the sensing experiments. YZ and DP contributed to the sensing data collection. All authors contributed to the analysis and discussion of the results. ZN and YS(*) wrote the manuscript, and all authors reviewed the manuscript. YS(*) supervised the project.

Coupling Aptazyme and Catalytic Hairpin Assembly for Cascaded Dual Signal Amplified Electrochemiluminescence Biosensing

Zhenqiang Ning, Yongjun Zheng, Deng Pan, Yuanjian Zhang and Yanfei Shen*

Medical School, School of Chemistry and Chemical Engineering, Southeast University, Nanjing 210009, China.

Email: Yanfei.Shen@seu.edu.cn

Abstract

Developing reliable and sensitive detection methods for adenosine triphosphate (ATP) is vital for both clinical diagnosis and food safety. In this work, by coupling aptazyme- and catalytic hairpin assembly (CHA)-based signal amplification and electrochemiluminescence (ECL), an ultrasensitive biosensor for sensing ATP was fabricated using $Ru(bpy)_3^{2+}$-doped silica nanoparticles ($RuSiO_2$) as ECL probes and a ferrocene-functionalized hairpin (hairpin-Fc) as quencher. The aptazyme-triggered cleavage of the DNA substrate and the CHA reaction both led to the circular release of trigger DNA, resulting in a significant dual signal amplification, with unprecedented enhancement up to 940-fold. Moreover, the bioconjugation of the DNA substrate with $Au@Fe_3O_4$ facilitated the separation and purification of the released trigger DNA, and effectively reduced the background signal. As a result, the as-prepared ECL biosensor exhibited a much lower detection limit of 0.054 pM for ATP, compared to those in previous reports, and showed high reliability for ATP detection in both spiked serum samples and *Staphylococcus aureus*. This work offers a new perspective for designing nucleic acid-based signal amplification for detecting ATP in bacterial analysis and clinical diagnosis.

Keywords:

adenosine triphosphate; aptazyme; $Ru(bpy)_3^{2+}$-doped silica nanoparticles; electrochemiluminescence; electron transfer

1. Introduction

As one of the most indispensable molecules in living organisms, adenosine triphosphate (ATP) plays an important role in numerous enzymatic activities and biological processes, the level of which, has a close relationship with some diseases and food sanitation(Dennis et al. 2001; Gourine et al. 2005; Liu et al. 2019b). As such, the concentrations of intercellular ATP have already been recognized as indicators of many diseases such as hypoglycemia, Parkinson's disease, ischemia and some malignant tumors(Gourine et al. 2005; Park et al. 2015). Moreover, since microbiological organisms like bacteria, yeast and mold also contain ATP, making detection of ATP widely explored in various foods and drinking water(Kim et al. 2018; Liu et al. 2019b; Vang et al. 2014). Thus, developing reliable and sensitive detection methods for ATP is of significant importance for both clinical diagnosis and food safety.

In the past few years, great efforts have been devoted to the development of various detection methods for ATP including high performance liquid chromatography, mass spectroscopy, fluorescence, chemiluminescence, and electrochemiluminescence (ECL)(Feng et al. 2019; Greenstein and Wert 2019; Zhang et al. 2019; Zhou et al. 2012). Among them, ECL has drawn increasing attentions in the fields of environmental monitoring (Hu et al. 2018; Li et al. 2019), food safety (Chen et al. 2018), clinical diagnosis (Sun et al. 2019b; Tang et al. 2013), and point-of-care testing (POCT) (Nie et al. 2019), because it couples the advantages of electrochemistry and chemiluminescence with prominent merits such as low background, high sensitivity

and simple-to-use equipment (Gong et al. 2019; Wang et al. 2019b). To achieve high sensitivity and wide dynamic range in practical assay, the integration of ECL technique with other recognition elements and analytical strategies are highly desirable.

Recently, aptazymes have gained intense interests because it not only inherit high specific recognition capacity of aptamers but also have DNAzyme-catalyzed signal amplification properties (Li et al. 2018; Liu and Lu 2004; Tang and Breaker 1997; Yang et al. 2016; Yousefi et al. 2018). Meanwhile, as an isothermal enzyme-free signal amplification method, catalytic hairpin assembly (CHA) can achieve exponential amplification of target DNA with negligible background at high speed (Dai et al. 2018; Jiang et al. 2013; Liu et al. 2019a). Although both the CHA- and aptazyme-based amplification have been proven to be feasible and public tools in various biosensors (Wang et al. 2019a), the coupling of CHA- and aptazyme-based amplification and ECL strategy for the detection of ATP has been rarely reported.

Herein, an efficient dual signal amplified ECL biosensor for ATP was designed by coupling an aptazyme-mediated reaction with CHA. The ATP-triggered aptazyme cleavage and CHA reactions resulted in the recycling of the aptazyme@ATP and trigger DNA, inducing significant signal amplification. Moreover, the DNA substrate was conjugated with $Au@Fe_3O_4$, which facilitated the separation and purification of the released trigger DNA. In addition, the utilization of $RuSiO_2$ instead of $Ru(bpy)_3^{2+}$ as an ECL probe further promoted the signal amplification, enhancing the sensitivity of the assay. The as-developed ECL biosensor exhibited a much lower detection limit

compared to those in previous reports, and was also applicable for ATP detection in both spiked serum samples and *Staphylococcus aureus* (*S. aureus*). It would offer a new perspective for the design of nucleic acid-based signal amplification tools for ATP biosensing.

2. Experimental Section

2.1 Preparation and modification of the $RuSiO_2$ nanoparticles

The $Ru(bpy)_3^{2+}$-doped silica nanoparticles ($RuSiO_2$) were prepared according to previous reports with some slight modifications (Ma et al. 2018; Sha et al. 2019). First, 1.77 mL of Triton X-100, 7.5 mL of cyclohexane and 1.8 mL of 1-hexanol were completely mixed by magnetic stirring. Then, 340 μL of 40 mM $Ru(bpy)_3^{2+}$ aqueous solution was slowly added and stirred for 30 min. Then, 100 μL of TEOS and 60 μL of $NH_3 \cdot H_2O$ were sequentially added into the mixture, and the reaction was continued for 24 h with magnetic stirring. Finally, 2 mL of acetone was used to destabilize the emulsion, and the $RuSiO_2$ nanoparticles were collected by centrifugation and rinsed with ethanol and water. To obtain amino group-functionalized $RuSiO_2$ ($RuSiO_2$-NH_2), 800 μL of APTES ethanol solution was used to react with 10 mL of 4 mg/mL $RuSiO_2$ for 8 h with magnetic stirring. The obtained $RuSiO_2$-NH_2 nanoparticles were resuspended in ultrapure water after washing with ethanol and water.

2.2 Preparation of $Au@Fe_3O_4$ nanoparticles and DNA-$Au@Fe_3O_4$ nanocomposites

Fe_3O_4-NH_2 nanoparticles were obtained through functionalization of Fe_3O_4

nanoparticles with APTES (see more details in Supporting Information). Au nanoparticles were synthesized by the following procedure (Frens 1973). In brief, 50 mL of 0.01% $HAuCl_4$ aqueous solution was heated to 100 °C, followed by adding 1 mL of 1% trisodium citrate. The above mixture was continuously heated for another 15 min. Then, 5 mg Fe_3O_4-NH_2 nanoparticles were added into 10 mL of the resulting Au nanoparticle solution with mechanical stirring overnight. The obtained Au/Fe_3O_4 nanohybrids (Au@Fe_3O_4) were collected by magnetic separation and redispersed in 5 mL of 0.1 M Tris-HCl buffer (pH 7.4).

For the functionalization of Au@Fe_3O_4 with a thiol-modified DNA substrate, 250 μL of 4 μM DNA substrate was mixed with 750 μL of the Au@Fe_3O_4 dispersion under mechanical stirring for 10 h. Then, 40 μL of 1 M NaCl was added to the solution, and this reaction was continued for 12 h. Finally, DNA-Au@Fe_3O_4 was obtained by magnetic separation and washing with 0.1 M Tris-HCl buffer. The products were redispersed in 500 μL of 0.1 M Tris-HCl buffer before use.

2.3 Construction of the ECL biosensor

Prior to use, the glassy carbon electrode (GCE) was polished with 0.3 μm alumina powder, followed by ultrasonic cleaning with ethanol and water three times, and then dried at room temperature. Subsequently, 5 μL of chitosan/$RuSiO_2$ mixture was dropped on the bare GCE, and the modified electrode was dried at room temperature. Next, the modified GCE was treated with 2.5% GA for 1 h. Next, the GCE was incubated with 10 μL of 2 μM capture DNA in PBS at 37 °C for 2 h. The capture DNA-modified GCE was then blocked with 20 μL of 10 μM DNA blocker for

2 h to avoid nonspecific binding. Finally, the ECL biosensor was obtained.

2.4 ECL sensing of ATP

A total of 100 μL of the DNA-Au@Fe_3O_4 dispersion was mixed with 10 μL of 4 μM aptazyme, and the mixture was then heated to 80 °C for 5 min and slowly cooled down to room temperature. During this process, the aptazyme will specifically bind to the DNA substrate in the DNA-Au@Fe_3O_4 to form aptazyme-DNA-Au@Fe_3O_4 based on the principle of Watson-Crick base pairing. Subsequently, the aptazyme-DNA-Au@Fe_3O_4 nanocomposite was incubated with 100 μL of ATP solution at different concentrations for 90 min. After magnetic separation, the precipitate was resuspended in 20 μL of 20 mM HEPES buffer containing 100 mM NaCl and 20 mM $MgCl_2$. The activated aptazyme digestion was allowed to proceed for 90 min, which generated significant amounts of trigger DNA fragments. The trigger DNA, separated by magnetic separation, was mixed with an equal volume of 4 μM hairpin-Fc by gentle vortexing. The designed ECL biosensor was incubated with this mixture at 37 °C for 90 min. Finally, the ECL of the resulting electrodes was measured in 0.1 M PBS buffer (pH 7.4) containing 25 mM TPA.

3. Results and Discussion

3.1 Principle of the proposed biosensor

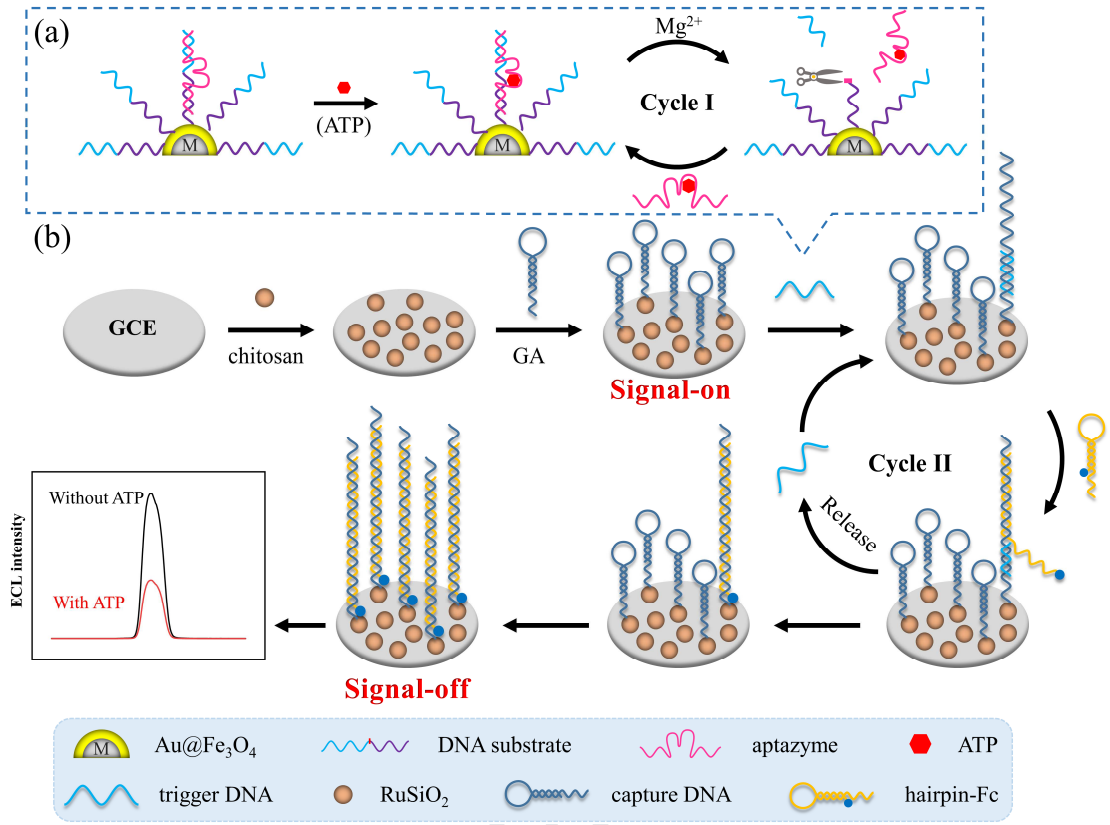

Figure 1. Schematic illustration of the construction and mechanism of the ECL biosensor for ATP detection. (a) Aptazyme-mediated signal amplification process. (b) Modification and detection procedure of the proposed ECL biosensor.

The construction of the ECL biosensor was based on a dual signal amplification strategy (Figure 1). As depicted in Figure 1, the added aptazyme hybridized with the DNA-Au@Fe_3O_4 nanocomposites, forming aptazyme-DNA-Au@Fe_3O_4. With the coexistence of ATP and Mg^{2+}, the aptazyme is activated and catalytically cleaves the DNA substrate, recycling the aptazyme@ATP hybrid, which leads to the release of an amplified amount of trigger DNA. Finally, the trigger DNA is facilely separated from the cleaved DNA-modified Au@Fe_3O_4 and purified by magnetic separation and then hybridized with the capture DNA on the electrode surface, inducing the CHA reaction,

i.e., the attachment of hairpin-ferrocene (Fc). As a result, the CHA reaction eventually generates a "capture DNA-hairpin-Fc" duplex. It should be noted that the formation of the "capture DNA-hairpin-Fc" duplex also results in the release and recycling of the trigger DNA, creating the secondary signal amplification. Moreover, the hybridization of the capture DNA and hairpin-Fc closed the distance between the Fc and the $RuSiO_2$ on the electrode surface, inducing a significant quenching of the ECL emission of the $RuSiO_2$ nanoparticles. Thus, the quenching of the ECL signal could be used to quantitate the detected ATP since the hairpin-Fc is quantitatively captured via the CHA reaction.

3.2 Preparation and characterization of the $RuSiO_2$ nanoparticles

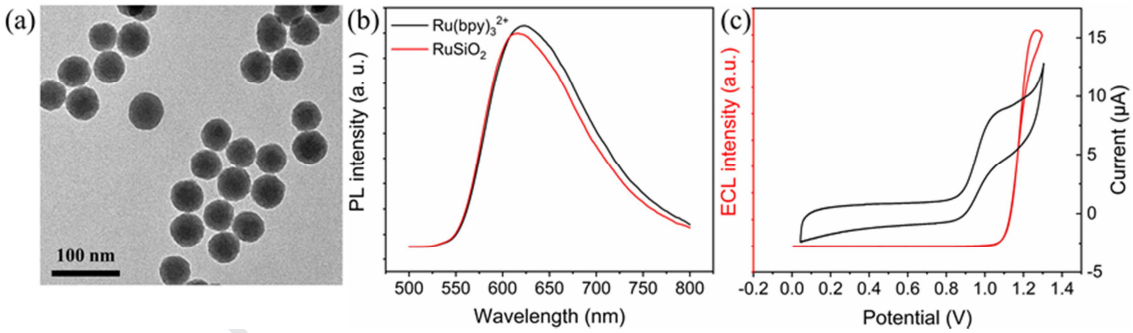

Figure 2. (a) TEM image of the $RuSiO_2$ nanoparticles. (b) Photoluminescence spectra of $Ru(bpy)_3^{2+}$ solution (black line) and $RuSiO_2$ nanoparticle dispersion (red line). The concentration of $Ru(bpy)_3^{2+}$ in the $Ru(bpy)_3^{2+}$ solution and $RuSiO_2$ nanoparticle dispersion were 5.0 μM and 3.2 μM (calculated according to the EDS results), respectively. λ_{ex}=453 nm. (c) The CV curve (black line) and ECL-potential curve (red line) of the $RuSiO_2$ nanoparticles. The ECL measurements were taken in 0.1 M PBS (pH 7.4) containing 25 mM TPA; PMT: 600 V, scan rate: 0.1 V/s.

The size and morphologies of the obtained $RuSiO_2$ nanoparticles were characterized by transmission electron microscopy (TEM). According to the TEM observations (Figure 2a), the as-prepared $RuSiO_2$ exhibited a uniform and monodispersed spherical shape with an average diameter of 50 nm. In addition, the elemental mapping results of $RuSiO_2$ showed that O, Si, Ru elements were uniformly distributed in the nanoparticles (Figure S1). As shown in Figure 2b, the PL spectrum of the $RuSiO_2$ nanoparticles was similar to that of $Ru(bpy)_3^{2+}$ with a slight blue-shift, which was possibly caused by the electrostatic interaction between $Ru(bpy)_3^{2+}$ and negatively charged SiO^- groups in silica oligomers, indicating that $Ru(bpy)_3^{2+}$ has been successfully doped into the SiO_2 matrix(Dang et al. 2014; Mirenda et al. 2013; Zhou et al. 2014).

The ECL performance and the electrochemical properties of $RuSiO_2$ nanoparticles were investigated by cyclic voltammetry (CV) in the potential range from 0 to 1.3 V in the presence of TPA (Figure 2c). To get insight in the ECL mechanism, the CV of the individual TPA and $Ru(bpy)_3^{2+}$ was also studied. As shown in Figure S2, the CV curve of TPA displayed an obvious oxidation peak with an onset potential at 0.78 V. Similarly, the $RuSiO_2$ exhibited an oxidation peak with a more positive onset potential at approximate 1.03 V. Meanwhile, the CV curve of the mixture of TPA and $RuSiO_2$ displayed an enhanced oxidation current with a similar onset potential with that of TPA, which might be the overlapping of the individual oxidation peak of TPA and $RuSiO_2$. At the same time, the ECL-potential curve of $RuSiO_2$/TPA in Figure 2c displayed an onset potential at approximate 1.04 V, which

was consistent with that of the CV curve of $RuSiO_2$ in Figure S2, suggesting that the ECL signal could be observed after the oxidation of TPA and $RuSiO_2$. As a result, the ECL-potential curve of $RuSiO_2$/TPA in Figure 2c showed a more positive onset potential, compared to the corresponding CV curve(Lu et al. 2018; Miao et al. 2002). Thus, all the results demonstrated that the $RuSiO_2$ nanoparticles was successfully prepared and could be applied as an excellent ECL probe for the construction of the ECL sensor.

3.3 Synthesis and characterization of the DNA-Au@Fe_3O_4 nanocomposite

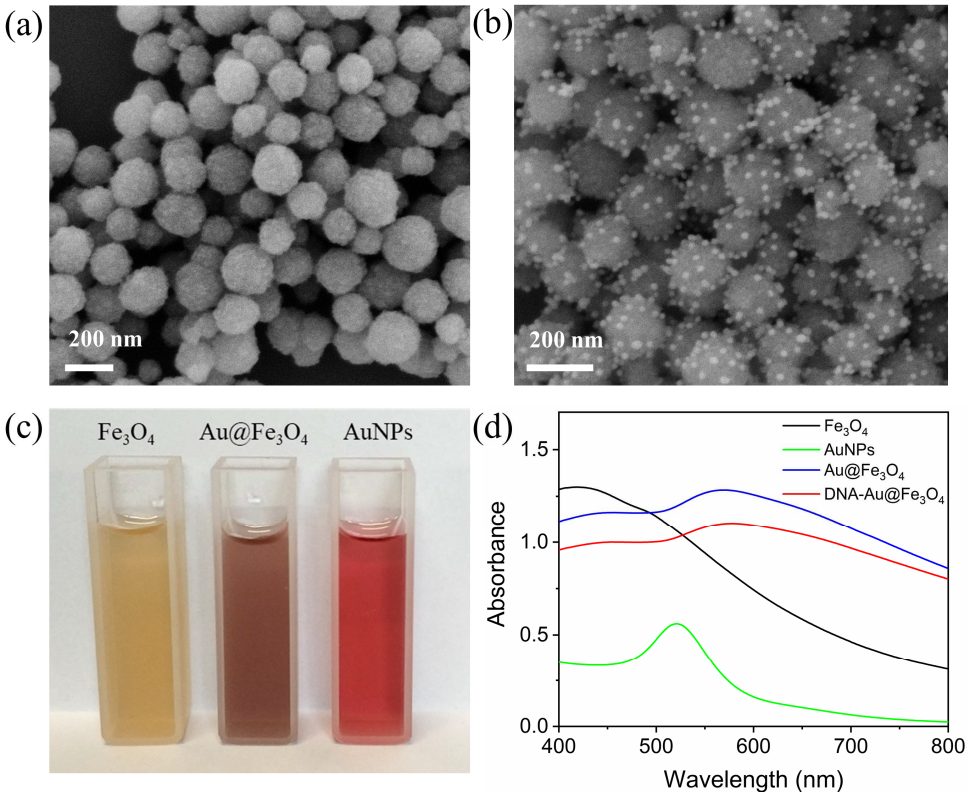

Figure 3. SEM characterization of (a) Fe_3O_4 and (b) Au@Fe_3O_4 nanoparticles. (c)The optical pictures of the Fe_3O_4, Au@Fe_3O_4 and Au NPs under natural light. (d) The UV-Vis absorbance spectra of the Fe_3O_4, Au NPs, and Au@Fe_3O_4 nanoparticles and

the DNA-Au@Fe_3O_4 nanocomposite.

The preparation of the Fe_3O_4 and the Au@Fe_3O_4 nanoparticles was first confirmed by TEM analysis. The TEM image of the Fe_3O_4 nanoparticles displayed a size distribution in the range of 150-200 nm with an average diameter of 175±29 nm (Figure 3a). After treatment with APTES, the pristine Fe_3O_4 was functionalized with amino-groups, which could be conjugated with Au NPs. As shown in Figure 3b, the SEM image of the Au@Fe_3O_4 nanoparticles showed that the Au NPs were uniformly distributed on the surface of the Fe_3O_4, allowing further functionalization of thiol-terminated DNA via the formation of Au-S bonds. The successful assembly of the Fe_3O_4 with Au NPs also resulted in a change in the solution color from yellow to reddish brown (Figure 3c). Accordingly, the UV-vis absorbance spectra of the Au@Fe_3O_4 nanoparticles presented a board surface plasmon resonance (SPR) peak of the Au NPs at 569 nm (Figure 3d)(Chowdhury et al. 2017). Compared to the absorption peak of the Au NPs at 520 nm, this red-shift could be attributed to the charge interference presented by the Fe_3O_4 nanoparticles(Jiang et al. 2016). After further functionalization with DNA, a slight red-shift was observed, indicating that the DNA substrate was successfully attached to the Au@Fe_3O_4 nanocomposite(Liu and Lu 2006).

3.4 Feasibility of the designed amplification system

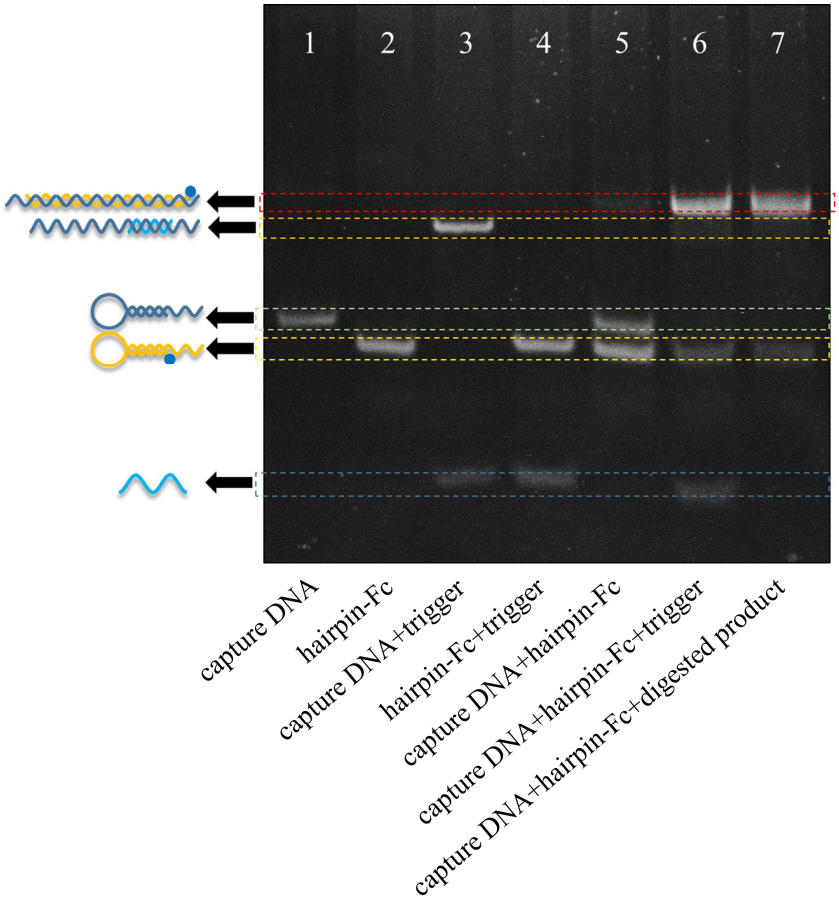

Figure 4. Feasibility analysis of the designed amplification systems by PAGE electrophoresis. Lane 1: capture DNA, lane 2: hairpin-Fc, lane 3: capture DNA + trigger DNA, lane 4: hairpin-Fc + trigger DNA, lane 5: capture DNA + hairpin-Fc, lane 6: capture DNA + hairpin-Fc + trigger DNA, lane 7: capture DNA + hairpin-Fc + digested product (produced through the designed aptazyme-mediated amplification systems incubating with 1 nM ATP). Equal volumes of 4 μM DNA were used in these experiments.

Before construction of the ECL biosensor, the feasibility of the designed amplification systems was assessed by PAGE electrophoresis analysis. As shown in Figure 4, a single band was observed in the lanes of the capture DNA and the

hairpin-Fc (Lane 1 and 2), indicating that the DNA fragments are a single component with high purity. The PAGE electrophoresis analysis of the hybridization reaction products showed that there was no new band when the capture DNA was mixed with hairpin-Fc, which confirmed that they cannot specifically bind to each other in the absence of the trigger DNA (lane 5). In contrast, a new band appeared upon the addition of the trigger DNA in the presence of the capture DNA (lane 3) because the trigger DNA can specifically bind with the exposed toehold domain of the capture DNA, initiating a branch migration that opens the hairpin. Owing to the exposure of the loop domain of the capture DNA with the sequences that are partly complementary to the toehold domain of the hairpin-Fc, the hairpin-Fc can initiate another branch migration that displaces the trigger DNA and finally forms a duplex of "capture DNA-hairpin-Fc". As expected, when commercial trigger DNA was added to the mixture of the capture DNA and hairpin-Fc, a new band was observed in lane 6 compared with those in lanes 3, 4 and 5. To confirm the feasibility and amplification effect of the designed system, the trigger DNA was separated from the products of the aptazyme-mediated enzymatic reaction initiated by adding 100 μL of 1 nM ATP solution. As shown in lane 7, a visible band of the "capture DNA-hairpin-Fc" duplex was observed, which indicated that the trace amounts of ATP successfully activated the designed amplification systems and generated significant amounts of the "capture DNA-hairpin-Fc" duplex. Interestingly, as the results show, approximately 0.940 μM duplex (estimated by *ImageJ* software, see more discussion in Figure S3) was eventually produced through the dual signal amplification strategy in response to 1

nM ATP, which implied the amplification time approximately 940-fold. All the above results suggest that efficient signal amplification can be achieved by taking advantage of the designed amplification systems.

3.5 Construction and characterization of the ECL biosensor

To confirm the stepwise fabrication of the ECL biosensor, CV and EIS characterization were performed. As shown in Figure S5a, the CV curve of the bare GCE exhibited a pair of well-defined reversible redox peaks. After coating the bare GCE with $RuSiO_2$ nanoparticles, the redox peak current decreased, implying poor conductivity of the $RuSiO_2$. A visible decrease of current responses and an increased peak potential difference were observed after incubation with capture DNA, which could be caused by the increased electron resistance and electronic repulsion between the negatively charged DNA and $[Fe(CN)_6]^{3-}$, demonstrating that capture DNA had been successfully immobilized onto the modified electrode. Similarly, the redox peak current further decreased upon the addition of the DNA blocker. The addition of the mixture of the trigger DNA and hairpin-Fc further induced a current reduction and enhanced peak potential difference, indicative of the formation of the capture DNA-hairpin-Fc duplex, which increased the steric hindrance and electronegativity on the electrode surface. In addition, the EIS results also confirmed the CV findings (shown in Figure S5b and Table S2). A small charge transfer resistance (R_{ct}) was found from the bare GCE, and the R_{ct} increased when the weakly conductive $RuSiO_2$ was coated to the electrode. After the modification of capture DNA and DNA blocker, the

R_{ct} values further increased, indicative of the successful assembly of capture DNA and DNA blocker on the electrode. Finally, the formation of the capture DNA-hairpin-Fc duplex on the electrode further resulted in an enhanced R_{ct} value. Therefore, both the CV and EIS results demonstrated that the proposed biosensor was successfully fabricated.

Furthermore, the ECL behavior of the stepwise modified electrodes was also investigated in 0.1 M PBS (pH 7.4) containing 25 mM TPA. As shown in Figure S6, an extremely weak ECL emission signal was observed for the bare GCE (curve a). As a result of the excellent luminous efficiency of $RuSiO_2$, the ECL intensity was remarkably enhanced after $RuSiO_2$ was coated onto the surface of the GCE (curve b). In contrast, after the modification of the capture DNA, the ECL intensity was decreased (curve c), owing to the capture DNA hindered charge transfer between the ECL probe and the coreactant. Similarly, the ECL intensity of the modified electrode was slightly decreased after the modification with the DNA blocker (curve d). Notably, the ECL intensity was sharply reduced when the hairpin-Fc hybridized with the capture DNA was placed on the electrode because of the quenching effect of the Fc on the ECL emission of $RuSiO_2$, indicating that the designed biosensor could be used for the ultrasensitive quantitative detection of ATP.

3.6 Quantitative detection of ATP

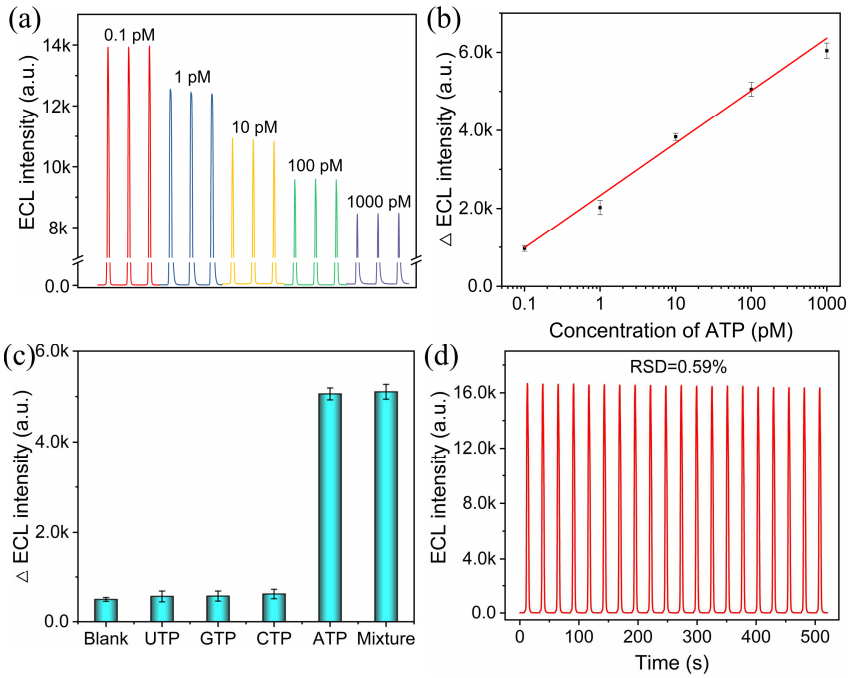

Figure 5. (a) The ECL intensities of this biosensor for different concentrations of ATP from 0.1 pM to 1000 pM. (b) Corresponding calibration curve of the △ECL intensity and the concentrations of ATP. (c) The specificity of the proposed biosensor toward ATP analogues. Concentrations of the ATP analogues and ATP were 100 pM. (d) The ECL signal stability of the proposed biosensor under consecutive scans for 20 cycles. The ECL measurements were performed in 0.1 M PBS (pH 7.4) containing 25 mM TPA, PMT: 800 V, scan rate: 0.1 V/s.

To assess the analytical performance of the designed ECL biosensor, the detection of various concentrations of ATP was quantified under optimized conditions (see more discussion in Figure S4). Figure 5a clearly shows that the ECL intensity gradually increased with increasing ATP concentration. The corresponding calibration curve (Figure 5b) exhibited a perfectly linear relationship between the decrease in the

ECL intensity (△ECL) and the logarithm of ATP concentration in the range from 0.1 pM to 1000 pM. The linear regression equation can be expressed as $\triangle ECL$=1343.69 lg c + 2331.64, with a correlation coefficient of 0.990 ($\triangle ECL$ and c represent the decrease of the ECL intensity and the concentration of ATP, respectively). Accordingly, the limit of detection (LOD) was calculated to be 0.054 pM. It should be noted that the conjugation of DNA substrate with Au@Fe_3O_4 facilitated the separation and purification of the released trigger DNA during the detection, and reduced the background signal (see more discussion in Figure S7). Furthermore, the comparison of analytical performance for the proposed biosensor and those reported previously was shown in Table 1, revealing the advantages of the proposed ECL biosensor with improved sensitivity and wide linear range. Therefore, the proposed dual signal amplified ECL biosensor is promising for the ultrasensitive detection of ATP.

Table 1. Comparison of previously reported analytical methods for detecting ATP

Method	Linear range (pM)	Detection limit (pM)	Reference
Colorimetric assay	1×10^4 - 6×10^5	1000	(Gao et al. 2017)
Fluorescence	1×10^2 - 1×10^5	80	(Ji et al. 2019)
Fluorescence	3×10^5 - 4×10^7	1.23×10^5	(Fan et al. 2018)
Electrochemistry	1×10^3 - 1×10^8	500	(Zhang et al. 2018)
Electrochemistry	1×10^3 - 2×10^5	600	(Li et al. 2018)
Photoelectrochemistry	5×10^3 - 3×10^6	2100	(Sun et al. 2019a)
Photoelectrochemistry	0.5 -5000	0.18	(Fan et al. 2016)

ECL	50 - 1×10^4	20	(Yao et al. 2009)
ECL	0.1-1000	0.054	This work

3.7 Specificity and stability of the designed ECL biosensor

The specificity and stability of the proposed biosensor were also assessed by selecting some ATP analogues, including UTP, GTP and CTP, as interfering agents. As shown in Figure 5c, the addition of UTP, GTP and CTP did not cause a significant ECL intensity change, which was similar with that of the blank sample. In the presence of ATP or a mixture of ATP and the interfering analogues, the $^{\triangle}$ECL intensity increased remarkably, implying high selectivity of the designed biosensor. Furthermore, the proposed biosensor also exhibited excellent stability of the ECL signals with a relative standard deviation (RSD) of 0.59% under consecutive scanning for 20 cycles (Figure 5d). Additionally, to further assess the stability, the biosensor treated with 100 pM ATP was stored at 4 °C in the dark, and 99.3%, 97.3%, 91.4% and 81% of the initial signal was preserved after storage for 1, 3, 7 and 14 days (Figure S8), respectively, indicating a satisfactory stability of the designed biosensor.

3.8 Preliminary application of real sample analysis

To evaluate the feasibility and reliability of the proposed biosensor for real sample analysis, quantitative detection of ATP in diluted human serums and *S. aureus* (ATCC 6538) were performed respectively. For the recovery experiment, ATP with different concentrations was spiked into 10% human serum and then detected by the

proposed ECL biosensor. As shown in Table S3, the recoveries were in the range of 95.68%-103.4%, demonstrating good reliability of this biosensor for real sample analysis. More importantly, ATP naturally existing in *S. aureus* was detected by this biosensor. The results in Figure S9 reveal that the intensity of $^{\triangle}$ECL intensity linearly increased with the number of *S. aureus* in the range from 10^3 cfu/mL to 10^6 cfu/mL. In addition, the ATP concentration obtained from the calibration curve shown in Figure 5 is consistent with the value reported previously(Hattori et al. 2003; Okanojo et al. 2017), indicating satisfactory accuracy of this biosensor for detecting ATP in natural samples.

4. Conclusions

In summary, we developed an efficient, sensitive and selective ECL biosensor for the detection of ATP by coupling aptazyme and CHA-based signal amplification technologies. The biological investigation showed that a 940-fold signal amplification could be obtained by the proposed nucleic acid-based signal amplification strategy. Moreover, the utilization of $RuSiO_2$ nanoparticles instead of $Ru(bpy)_3^{2+}$ as ECL probes further promoted the signal amplification, enhancing the sensitivity of the assay. In addition, the bioconjugation of DNA substrate with $Au@Fe_3O_4$ facilitated the separation and purification of the released trigger DNA, and effectively reduced background signal. The proposed ECL biosensor exhibited promising sensing performance for both spiked serum samples and *S. aureus*. This work might provide a new ECL-based signal amplification strategy for ATP detection in both food safety

and clinical diagnostics.

Conflicts of interest

There are no conflicts of interest to declare.

Acknowledgements

This work is supported by the National Natural Science Foundation of China (21675022 and 21775018), the Program from the Natural Science Foundation of Jiangsu Province (BK20170084 and BK20160028), the Fundamental Research Funds for the Central Universities (2242019K3DN04 and 2242019K41036) and Postgraduate Research & Practice Innovation Program of Jiangsu Province (KYCX19_0119).

References

Chen, M.M., Wang, Y., Cheng, S.B., Wen, W., Zhang, X., Wang, S., Huang, W.H., 2018. Anal. Chem. 90 (8), 5075-5081.

Chowdhury, A.D., Agnihotri, N., Doong, R., De, A., 2017. Anal. Chem. 89 (22), 12244-12251.

Dai, W., Zhang, J., Meng, X., He, J., Zhang, K., Cao, Y., Wang, D., Dong, H., Zhang, X., 2018. Theranostics 8 (10), 2646.

Dang, J., Guo, Z., Zheng, X., 2014. Anal. Chem. 86 (18), 8943-8950.

Dennis, P.B., Jaeschke, A., Saitoh, M., Fowler, B., Kozma, S.C., Thomas, G., 2001. Science 294 (5544), 1102.

Fan, G.C., Zhao, M., Zhu, H., Shi, J.J., Zhang, J.R., Zhu, J.J., 2016. J. Phys. Chem. C 120 (29), 15657-15665.

Fan, Y., Mou, Z., Wang, M., Li, J., Zhang, J., Dang, F., Zhang, Z., 2018. Anal. Chem. 90 (22), 13708-13713.

Feng, G., Zhang, B., Wang, S., Ding, Z., Li, G., Zhang, X., 2019. Sens. Actuator

B-Chem. 301, 127090.

Frens, G., 1973. Nature Phys. Sci. 241 (105), 20-22.

Gao, Z., Qiu, Z., Lu, M., Shu, J., Tang, D., 2017. Biosens. Bioelectron. 89, 1006-1012.

Gong, Z., Zheng, W., Gao, Y., Huang, P., Tu, D., Li, R., Wei, J., Zhang, W., Zhang, Y., Chen, X., 2019. Angew. Chem.-Int. Edit. 58 (21), 6943-6947.

Gourine, A.V., Llaudet, E., Dale, N., Spyer, K.M., 2005. Nature 436 (7047), 108-111.

Greenstein, K.E., Wert, E.C., 2019. Water Res. 154, 171-179.

Hattori, N., Sakakibara, T., Kajiyama, N., Igarashi, T., Maeda, M., Murakami, S., 2003. Anal. Biochem. 319 (2), 287-295.

Hu, Y., Liu, Z., Zhan, H., Shen, Z., 2018. Anal. Methods 10 (7), 767-774.

Ji, X., Wang, J., Niu, S., Ding, C., 2019. Chem. Commun. 55 (36), 5243-5246.

Jiang, G., Huang, Y., Zhang, S., Zhu, H., Wu, Z., Sun, S., 2016. Nanoscale 8 (41), 17947-17952.

Jiang, Y.S., Li, B., Milligan, J.N., Bhadra, S., Ellington, A.D., 2013. J. Am. Chem. Soc. 135 (20), 7430-7433.

Kim, S.U., Jo, E.-J., Noh, Y., Mun, H., Ahn, Y.-D., Kim, M.-G., 2018. Anal. Chem. 90 (17), 10171-10178.

Li, S., Li, J., Ma, X., Pang, C., Yin, G., Luo, J., 2019. Biosens. Bioelectron. 139, 111321.

Li, X., Yang, J., Xie, J., Jiang, B., Yuan, R., Xiang, Y., 2018. Biosens. Bioelectron. 102, 296-300.

Liu, J., Lu, Y., 2004. Anal. Chem. 76 (6), 1627-1632.

Liu, J., Lu, Y., 2006. Nat. Protoc. 1 (1), 246-252.

Liu, J., Zhang, Y., Xie, H., Zhao, L., Zheng, L., Ye, H., 2019a. Small 15 (42), 1902989.

Liu, Z., Zhong, Y., Hu, Y., Yuan, L., Luo, R., Chen, D., Wu, M., Huang, H., Li, Y., 2019b. Food Chem. 270, 573-578.

Lu, H.J., Pan, J.B., Wang, Y.Z., Ji, S.Y., Zhao, W., Luo, X.L., Xu, J.J., Chen, H.Y., 2018. Anal. Chem. 90 (17), 10434-10441.

Ma, J., Wu, L., Li, Z., Lu, Z., Yin, W., Nie, A., Ding, F., Wang, B., Han, H., 2018. Anal. Chem. 90 (12), 7415-7421.

Miao, W., Choi, J., Bard, A.J., 2002. J. Am. Chem. Soc. 124 (48), 14478-14485.

Mirenda, M., Levi, V., Bossi, M.L., Bruno, L., Bordoni, A.V., Regazzoni, A.E., Wolosiuk, A., 2013. J. Colloid Interface Sci. 392, 96-101.

Nie, Y., Liu, Y., Zhang, Q., Su, X., Ma, Q., 2019. Biosens. Bioelectron. 138, 111318.

Okanojo, M., Miyashita, N., Tazaki, A., Tada, H., Hamazoto, F., Hisamatsu, M., Noda, H., 2017. Luminescence 32 (5), 751-756.

Park, J., Byun, J., Shim, W., Kim, S.U., Kim, M., 2015. Biosens. Bioelectron. 73, 26-31.

Sha, H., Zhang, Y., Wang, Y., Ke, H., Xiong, X., Xue, H., Jia, N., 2019. Biosens. Bioelectron. 132, 203-209.

Sun, J., Li, L., Kong, Q., Zhang, Y., Zhao, P., Ge, S., Cui, K., Yu, J., 2019a. Biosens. Bioelectron. 133, 32-38.

Sun, M.F., Liu, J.L., Chai, Y.Q., Zhang, J., Tang, Y., Yuan, R., 2019b. Anal. Chem. 91 (12), 7765-7773.

Tang, J., Breaker, R.R., 1997. Chem. Biol. 4 (6), 453-459.

Tang, X., Zhao, D., He, J., Li, F., Peng, J., Zhang, M., 2013. Anal. Chem. 85 (3), 1711-1718.

Vang, Ó.K., Corfitzen, C.B., Smith, C., Albrechtsen, H., 2014. Water Res. 64, 309-320.

Wang, S., Lu, S., Zhao, J., Ye, J., Huang, J., Yang, X., 2019a. Biosens. Bioelectron. 126, 565-571.

Wang, X., Shang, L., Zhang, W., Jia, L.P., Ma, R.N., Jia, W.L., Wang, H.S., 2019b. Biosens. Bioelectron. 141, 111436.

Yang, Y., Huang, J., Yang, X., Quan, K., Wang, H., Ying, L., Xie, N., Ou, M., Wang, K., 2016. Anal. Chem. 88 (11), 5981-5987.

Yao, W., Wang, L., Wang, H., Zhang, X., Li, L., 2009. Biosens. Bioelectron. 24 (11), 3269-3274.

Yousefi, H., Ali, M.M., Su, H.-M., Filipe, C.D.M., Didar, T.F., 2018. ACS Nano 12 (4), 3287-3294.

Zhang, X., Song, C., Yang, K., Hong, W., Lu, Y., Yu, P., Mao, L., 2018. Anal. Chem. 90 (8), 4968-4971.

Zhang, X., Wang, Y., Zhou, X., 2019. Anal. Chem. 91 (2), 1665-1670.

Zhou, L., Huang, J., Yang, L., Li, L., You, T., 2014. Anal. Chim. Acta 824, 57-63.

Zhou, L., Xue, X., Zhou, J., Li, Y., Zhao, J., Wu, L., 2012. J. Agric. Food. Chem. 60 (36), 8994-8999.

Highlights:

- Aptazyme- and CHA-based signal amplification was coupled with ECL for biosensing of ATP.
- The aptazyme- and CHA-based signal amplification resulted in an enhancement up to 940-fold.
- The detection was based on the electron transfer between $RuSiO_2$ probes and Fc quenchers.
- Anchoring DNA on $Au@Fe_3O_4$ facilitated separation and purification of the released trigger DNA.
- The biosensor showed high reliability for both spiked serum samples and Staphylococcus aureus.

ZN and YS(*), conceived and planned experiments. ZN prepared the nanocomposites, and performed the sensing experiments. YZ and DP contributed to the sensing data collection. All authors contributed to the analysis and discussion of the results. ZN and YS(*) wrote the manuscript, and all authors reviewed the manuscript. YS(*) supervised the project.

Declaration of interests

☒ The authors declare that they have no known competing financial interests or personal relationships that could have appeared to influence the work reported in this paper.

☐The authors declare the following financial interests/personal relationships which may be considered as potential competing interests: